


# SCIENTIFIC REPORTS



OPEN

## MoS<sub>2</sub> Surface Structure Tailoring via Carbonaceous Promoter

Yumeng Shi<sup>1,\*</sup>, Henan Li<sup>2,\*</sup>, Jen It Wong<sup>1,\*</sup>, Xiaoting Zhang<sup>3</sup>, Ye Wang<sup>1</sup>, Huaihe Song<sup>3</sup> & Hui Ying Yang<sup>1</sup>

Received: 05 January 2015

Accepted: 13 March 2015

Published: 21 May 2015

Atomically thin semiconducting transition-metal dichalcogenides have been attracting lots of attentions, particularly, molybdenum disulfide (MoS<sub>2</sub>) monolayers show promising applications in field effect transistors, optoelectronics and valleytronics. However, the controlled synthesis of highly crystalline MoS<sub>2</sub> remain a challenge especially the systematic approach to manipulate its structure and morphology. Herein, we report a method for controlled synthesis of highly crystalline MoS<sub>2</sub> by using chemical vapor deposition method with carbonaceous materials as growth promoter. A uniform and highly crystalline MoS<sub>2</sub> monolayer with the grain size close to 40 μm was achieved. Furthermore, we extend the method to the manipulation of MoS<sub>2</sub> morphology, flower-shape vertical grown MoS<sub>2</sub> layers were obtained on growth promoting substrates. This simple approach allows an easy access of highly crystalline MoS<sub>2</sub> layers with morphology tuned in a controllable manner. Moreover, the flower-shape MoS<sub>2</sub> grown on graphene oxide film used as an anode material for lithium-ion batteries showed excellent electrochemical performance.

Direct bandgap semiconducting transition metal dichalcogenide (TMD) monolayers are attractive for optoelectronics and energy harvesting<sup>1,2</sup>. Their high carrier mobility<sup>3</sup>, excellent on-off ratio<sup>4</sup> and good bendability<sup>5</sup> are promising for future flexible and low-power consumer electronics<sup>5,6</sup>. The fundamental studies on their electronic structures and valley-spin relations are also emerging<sup>7,8</sup>. Being a member of the TMDs family, molybdenum disulfide (MoS<sub>2</sub>) has already attracted considerable attention for its great potential in the fields of hydrogen evolution reaction (HER)<sup>9,10</sup>, bio-sensing<sup>11,12</sup> and energy storage<sup>13–15</sup>. Recently, it has been demonstrated that ultra-thin MoS<sub>2</sub> crystals with a typical thickness of ~0.65 nm holds even more significant promise in electronics<sup>4,16,17</sup> and optoelectronics<sup>7,18–22</sup>.

Given the great promises hold, it is highly desirable to develop a scalable method to obtain large-area and high quality TMD monolayers. On the other hand, controlling the surface structure of MoS<sub>2</sub> layers at the atomic scale is also critical for their successful implementation in each applications. For example, large specific surface areas are preferred for the energy storage application<sup>13,14</sup>. For the application of HER, only the edge sites of MoS<sub>2</sub> are catalytically active, which require the controllable synthesis of MoS<sub>2</sub> layers with abundant exposed edge sites<sup>10,23</sup>. Recently, chemical vapor deposition (CVD) method has led towards high-quality TMD layers with scalable size, controllable thickness and excellent electronic properties. Several groups have made remarkable progress in MoS<sub>2</sub> synthesis<sup>8,24–26</sup>. Among the various approaches for MoS<sub>2</sub> synthesis, those using MoO<sub>3</sub> and sulfur powder as solid state precursors become dominant<sup>26–30</sup>, which is due to the simplified process and high yield of monolayers.

However, it is more challenging to grow single crystalline monolayer MoS<sub>2</sub> thin film by CVD method comparing to other 2D materials synthesis such as graphene<sup>31,32</sup> and boron nitride<sup>33,34</sup>, where catalyst were used to control the geometry, thickness and crystallinity. In contrast, the growth of MoS<sub>2</sub> by CVD does not involve any catalysts<sup>35,36</sup> and the growth of MoS<sub>2</sub> is very sensitive to the substrate treatment prior to the growth<sup>18,22</sup>. Previous reports demonstrate nucleation of MoS<sub>2</sub> can be facilitated by seeding

<sup>1</sup>Pillar of Engineering Product Development, Singapore University of Technology and Design, Singapore 487372.

<sup>2</sup>Nanyang Technological University, School of Materials Science and Engineering, 50 Nanyang Avenue, Singapore 639798.

<sup>3</sup>State Key Laboratory of Chemical Resource Engineering, Beijing University of Chemical Technology, Beijing 100029.

\*These authors contributed equally to this work. Correspondence and requests for materials should be addressed to H.Y.Y. (email: yanghuiying@sutd.edu.sg)

the substrate with graphene-like species<sup>29,30,37</sup>. Meanwhile Najmaei *et al.* have shown that the MoS<sub>2</sub> crystallines commonly nucleate on the step edges during growth without the present of seeding molecules<sup>28</sup>. Recently, Van der Zande *et al.* proved that large MoS<sub>2</sub> crystalline islands can be obtained by using ultraclean substrates and fresh precursors and neither seeding molecules nor step-edge were used to promote the nucleation of MoS<sub>2</sub><sup>27</sup>. It was suggested that the MoS<sub>2</sub> growth normally follows an analogous layer-plus-island (or Stranski-Krastanov) growth mode<sup>8</sup>. The Stranski-Krastanov mode is a two-step process: initially, monolayer MoS<sub>2</sub> domains gather and interconnect with each other till the full coverage of monolayer is nearly completed. Beyond the critical layer number (1 for MoS<sub>2</sub>), the growth of MoS<sub>2</sub> continues through the nucleation and coalescence of MoS<sub>2</sub> nanoparticles or few layers islands<sup>8</sup>. In other words, the thermodynamics favors the basal plane growth, which limits the tunability of surface structure.

Nevertheless, the widely used method for MoS<sub>2</sub> synthesis is based on the direct chemical vapor phase reaction of MoO<sub>3</sub> by S gas in which the MoO<sub>x</sub> vapor generated from MoO<sub>3</sub> powder reacts with sulfur vapor at elevated temperatures to form monolayer MoS<sub>2</sub> on the collecting substrates<sup>26,29</sup>. Thus, it is common to obtain molybdenum oxide microcrystals byproducts since the reduction of MoO<sub>3</sub> also produce MoO<sub>2</sub> crystals under similar growth condition<sup>38</sup>. MoO<sub>3</sub> was selected by Li *et al.* as a precursor for MoS<sub>2</sub> growth on the basis that it has an evaporation temperature of ~700 °C<sup>26</sup>. However, the growth dynamics of MoO<sub>3-x</sub> and S are still not fully understood. It has been suggested in literatures<sup>39,40</sup> that there are two channels for MoO<sub>3-x</sub> to react with S, one is it adsorb and diffuse on the substrate, reacting with S to form MoS<sub>2</sub>; the other is forming MoS<sub>2</sub> clusters in vapour phase and crystalize on substrate. Both these two channels require the forming of vapour phase MoO<sub>3-x</sub>; and the growth temperature ranging from 530 °C to 850 °C. Thus far, it is demanding to have a better understanding of the growth mechanism and further develop a method which is capable of producing large monolayer MoS<sub>2</sub> crystals, preventing the formation of MoO<sub>2</sub> byproducts, meanwhile controlling the surface structure of MoS<sub>2</sub> layers at the atomic scale.

Herein, we engineer the reduction process of MoO<sub>3</sub> precursor by carbon based materials. In a typical synthesis, the solid state precursor of MoO<sub>3</sub> powder is covered by a piece of carbon cloth. The carbon cloth is chosen simply due to its thermal stability, good mechanical property and micro porous structure. MoO<sub>3</sub> powder can be thermally evaporated and only the gas phase MoO<sub>3</sub> can pass through the opening of woven micro carbon fibers and it is then reduced by sulfur vapor at 650 to 700 °C. It was found that carbon can help reducing MoO<sub>3</sub> and large MoO<sub>2</sub> crystals can be trapped by the carbon cloth which effectively prevents the co-deposition of MoO<sub>2</sub> and MoS<sub>2</sub> on the collecting substrates. Finally, continuous large-area MoS<sub>2</sub> thin films was successfully grown on substrate. The synthesized MoS<sub>2</sub> layers are in a well-defined triangular shape with a typical lateral size ~40 μm. We further investigated the effects of carbonaceous promoter in the growth of MoS<sub>2</sub> on various substrates. By simply replacing the SiO<sub>2</sub>/Si substrates with GO film or GO flakes, few-layer MoS<sub>2</sub> preferentially form on the surface of GO under the same growth condition. The results suggest, the growth of MoS<sub>2</sub> is very sensitive to the substrate treatment and carbon based materials can significantly promote the growth rate and yield of MoS<sub>2</sub>, which is due to the assisted reduction of MoO<sub>3</sub> by carbon.

This work elucidates how morphological control of MoS<sub>2</sub> at the nanoscale can be achieved by carbonaceous promoter. The surface morphology engineering of MoS<sub>2</sub> layers enables new opportunities for enhancing surface properties for catalysis, energy storage and other important technological applications. As a proof-of-concept, the MoS<sub>2</sub>/GO composites were used as electrode materials to demonstrate its application in lithium ion batteries (LIBs). The surface structure engineering of MoS<sub>2</sub>/GO provides highly efficient pathways for both electronic and Li ion exchange during the charge/discharge cycles of the battery, which allows the composite to be directly used as working electrode and assembled into a coin cell without adding any conductive or binder materials. A remarkably high specific capacity (i.e., > 1000 mAh g<sup>-1</sup>) was achieved at the current density of 100 mA g<sup>-1</sup>, which is much higher than theoretical value for either GO or MoS<sub>2</sub> alone (~566 and ~670 mAh g<sup>-1</sup>, respectively). The MoS<sub>2</sub>/GO composites also show an outstanding high-rate charge/discharge performance. Even at a very high current density of 1000 mA g<sup>-1</sup>, the composite electrode can still deliver a capacity of 776 mAh g<sup>-1</sup> after 500 cycles. The reversible capacity only slightly decreases to 727 mAh g<sup>-1</sup> after an additional 440 cycles under 2000 mA g<sup>-1</sup>. The high rate capability can be attributed to the unique nano-architecture engineering of MoS<sub>2</sub>, which provides structural stability and transport advantages for both electrons and lithium ions.

## Materials and Methods

**Monolayer CVD-MoS<sub>2</sub> growth.** CVD-MoS<sub>2</sub> was prepared using chemical vapor deposition method with carbon based materials as a growth promoter. High-crystal-quality MoS<sub>2</sub> can be grown on a silicon substrate with 300 nm SiO<sub>2</sub> layer on top inside a hot-wall horizontal tube furnace. To be brief, the MoS<sub>2</sub> films were synthesized using high purity MoO<sub>3</sub> (99%, Aldrich) and S powder (99.5, Sigma-Aldrich) as precursors. The precursors were placed in two separated Al<sub>2</sub>O<sub>3</sub> crucibles and the substrates were placed on the downstream side of the Ar carrying gas. A piece of carbon cloth was put on top of MoO<sub>3</sub> powder for better growth control. The growth chamber was firstly heated to 105 °C with Ar flow rate of 1000 sccm, this step helps to remove the oxygen and moistures in the chamber. After that, the temperature was further increase to 700 °C with a heating rate of 15 °C/min. MoS<sub>2</sub> monolayer in a triangle shape were obtained by annealing at 700 °C for 10 min followed by a naturally cooling process to room temperature. Ar flow rate was kept at 10 sccm during MoS<sub>2</sub> growth.

**Flower shape MoS<sub>2</sub> growth.** Before the CVD synthesis, 1 mg/ml Graphene oxide (GO) dispersion in water was obtained after 30 min probe sonication of GO flakes (Graphene Supermarket, USA.) in deionized water (DI Water). The 300 W probe sonicator was set at 30% amplitude with alternating pulse. GO coated Si substrate was prepared by drop casting GO dispersion on a piece of cleaned SiO<sub>2</sub>/Si substrates and gently blow dried using N<sub>2</sub> gas. Self-supporting GO thin film was obtained by vacuum filtration of GO dispersion with a polymer filter membranes (pore size 0.02 μm, GE Whatman, USA). The filtration membrane was further removed by dissolving it in hot Acetone solution (at ~80 °C). The GO substrates were carried into the growth chamber after baking on hot plate at 90 °C for 1 hour to remove organic solvent and water. The growth condition was kept the same as monolayer MoS<sub>2</sub> synthesis.

**Chemicals and precursors.** Graphene oxide powder was purchased from Graphene Supermarket, Calverton, NY, USA. MoO<sub>3</sub> (purity 99%) and S powder (purity 99.5%) powder purchased from Sigma-Aldrich Co. (Singapore) were directly used for MoS<sub>2</sub> synthesis without further purification. Carbon cloth was purchased from Hesen Shanghai Co., Ltd, China.

**MoS<sub>2</sub>/GO transfer for TEM characterization.** The CVD synthesized MoS<sub>2</sub>/GO composite was transferred by coating the film with a thin layer (~100 nm) of Poly[methylmethacrylate] (PMMA). After etching the underlying SiO<sub>2</sub>/Si substrates with NaOH aquariums (with a concentration of 3 M) at 80 °C, the PMMA/ MoS<sub>2</sub>/GO film was transferred to DI water and was suspended on the surface of water to remove the etchant residue for several hours. Subsequently, the film can be transferred to any substrate or TEM grids for analysis and characterization. Finally, the top layer of PMMA can be removed by acetone or by directly annealing the samples in an Ar and H<sub>2</sub> atmosphere at 450 °C for 2 hours.

**Raman measurements.** The Raman measurements were carried out using a WITec alpha 300 confocal Raman microscope. The Raman spectra presented in this paper were collected using a 532 nm solid-state laser for excitation with the beam focused by a 100X objective lens. The laser beam diameter on sample is around 500 nm. Scanning electron microscopy (SEM) was performed on a field emission SEM (FESEM) instrument (JSM-7600F, Japan). A field-emission transmission electron microscope (JEOL JEM-2100F, operated at 200 keV), equipped with an energy dispersive spectrometer (EDS) was used to obtain the information of the microstructures and the chemical compositions.

**Electrochemical measurement.** The electrochemical performance of MoS<sub>2</sub>/GO nanocomposites electrode was measured with a half-cell lithium ion battery (LIBs) configuration. The 2032 coin-type cells were assembled in an argon-filled glove-box with both the moisture and oxygen level less than 0.5 ppm. MoS<sub>2</sub>/GO composites were directly used as cathodes. For control samples, the working electrode materials of GO and MoS<sub>2</sub> were prepared by mix GO and MoS<sub>2</sub> powders with a certain weight percentage in solution phase and then freeze-dried to form a self-supporting membrane. Lithium sheet was used as anodes and 1 M LiPF<sub>6</sub> in a 1/1 (volume ratio) mixture of ethylene carbonate (EC)/dimethyl carbonate (DMC) as electrolyte. Celgard® 2400 was used as the separator of the battery. The cells were tested on a NEWARE multi-channel battery test system with galvanostatic charge and discharge in the voltage range between 0.01 and 3.0 V vs. Li/Li<sup>+</sup> at various current density at room temperature. The cyclic Voltammetry (CV) and electrochemical impedance spectroscopy (EIS) were tested on an electrochemical workstation (VMP3, Bio-Logic).

## Results and Discussion

**Effect of carbon based materials on monolayer MoS<sub>2</sub> growth.** A schematically illustration of the experimental set-up used for MoS<sub>2</sub> synthesis is presented in Fig. 1 (a). MoS<sub>2</sub> monolayers were grown by CVD with solid MoO<sub>3</sub> and S precursors. In contrast to previous reports, the MoO<sub>3</sub> powder with a weight of ~15 mg was directly placed on a silicon wafer which is next to the collecting substrates for MoS<sub>2</sub> growth. A piece of carbon cloth (thickness: 0.34 ± 0.02 mm, surface area ~50 mm<sup>2</sup>) was put on the top of MoO<sub>3</sub> powder. Prior to the growth, argon gas was used to flush the quartz tube thoroughly in order to remove the oxygen and moistures. 10 sccm of argon was supplied during the synthesis of MoS<sub>2</sub> monolayers, while the growth chamber was heated from room temperature to 700 °C with a temperature profile as shown in Fig. 1 (a).

Detailed growth procedure can be found in the method section. At such temperature, MoO<sub>3</sub> powder evaporated and reacted with sulfur vapor to form a continuous MoS<sub>2</sub> films and isolated triangular MoS<sub>2</sub> domains can also be found at the edges along the film which are shown in the optical microscopy images (with different magnifications) of Fig. 1 (b), (c) and (d) where the MoS<sub>2</sub> sheets were grown on the SiO<sub>2</sub>/Si substrate. The triangular shape of the crystallites reflects the 3-fold symmetry of MoS<sub>2</sub> that suggests they are single-crystalline<sup>30,41</sup>. Similar to previous work, the monolayer MoS<sub>2</sub> can be merged to form a large MoS<sub>2</sub> sheet<sup>29</sup>, and among different growths the average size of MoS<sub>2</sub> islands varies between 10 to 40 μm. The intensity of photoluminescence (PL) peak and the energy separation between the Raman A<sub>1g</sub> and E<sub>2g</sub> peaks have been found related to the number of MoS<sub>2</sub> Layers<sup>42–44</sup>. Therefore, Raman and PL measurement were carried out to confirm the quality of the individual crystallites. Fig. 1 (e) and (f) show the PL intensity mapping and the corresponding intensity mapping of Raman peak of an isolated triangular MoS<sub>2</sub> crystallite. Figure 1 (g) displays the typical spectra taken from the MoS<sub>2</sub> crystallite that consisting

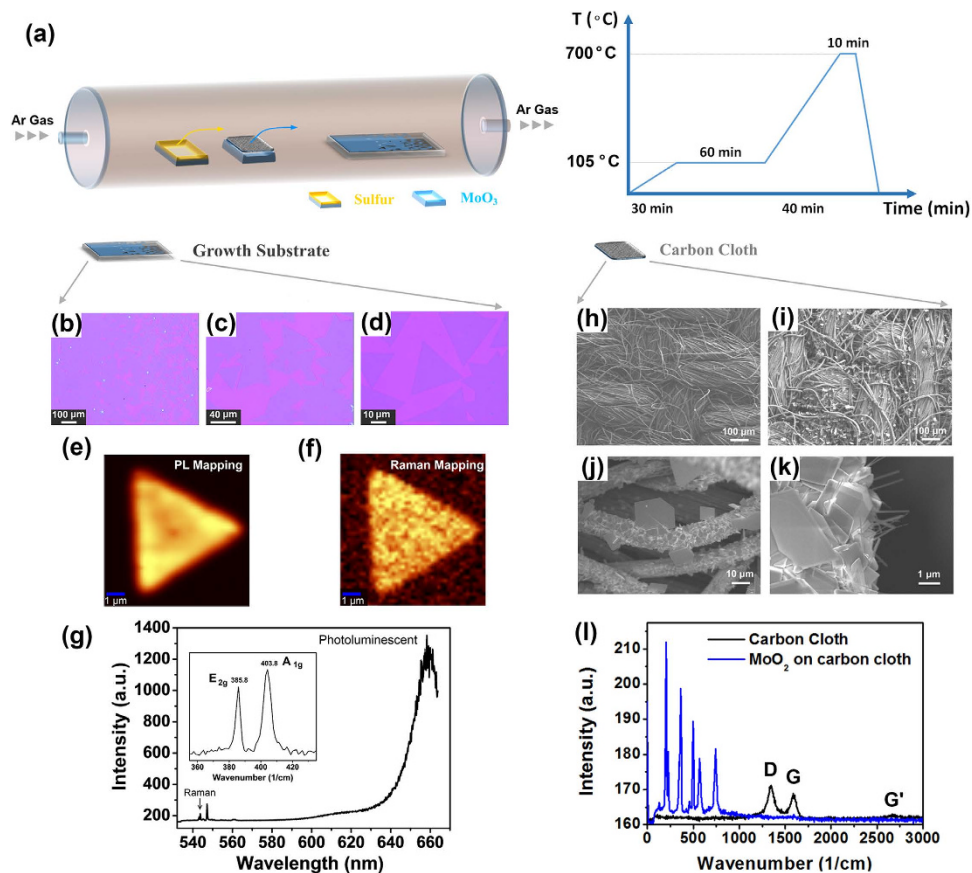


**Figure 1.** (a) Schematic illustration of the experimental set-up for CVD-growth of MoS<sub>2</sub>; and illustration of temperature profile for the MoS<sub>2</sub> growth process at different stages. (b), (c) and (d) show the optical images for as-grown MoS<sub>2</sub> monolayer films and isolated monolayer crystallites. (e) Photoluminescence (PL) map of the synthesized MoS<sub>2</sub> monolayers, and (f) shows the corresponding Raman intensity map. The synthesized MoS<sub>2</sub> were grown on SiO<sub>2</sub>/Si substrates. (g) Experimental results show the PL spectrum of MoS<sub>2</sub> films. Inset, typical Raman spectra collected from the area of the MoS<sub>2</sub> monolayer film. (h) and (i) SEM images of carbon cloth surface before and after CVD process; (j) and (k) SEM images show large crystals can be found on carbon cloth surface; (l) Raman spectrum taken from the pristine carbon cloth and the one after CVD synthesis.

both the Raman and PL peaks. The strong PL peak and high PL to Raman intensity ratio suggest the direct band gap photoluminescence. The inset figure in Fig. 1 (g) presents the Raman peak of monolayer MoS<sub>2</sub>, the E<sub>2g</sub> and A<sub>1g</sub> peaks locate at 385.8 and 403.8 cm<sup>-1</sup>, respectively with a peak distance of 18 cm<sup>-1</sup>. The small E<sub>2g</sub> and A<sub>1g</sub> peak distance suggests the monolayer nature of these MoS<sub>2</sub> crystallites<sup>45,46</sup>.

We note that without the carbon cloth, triangular shape MoS<sub>2</sub> can also be obtained but there will be few-layer MoS<sub>2</sub> and/or MoO<sub>2</sub> crystallites distributed among them, as shown in Supporting Data (Fig. S1). As a consequence, under our growth condition, carbon based materials play an important role in facilitating the monolayer MoS<sub>2</sub> growth. It is worthy to mention that, recently reports demonstrated aromatic molecules are helpful for the nucleation of the MoS<sub>2</sub> layers<sup>29,30</sup>. However, it is still controversial that a larger single layer MoS<sub>2</sub> can be obtained by using carefully cleaned substrates<sup>27,28</sup>. In this study, the carbon cloth is separated from the collecting substrates, and pre-annealed at 700 °C to exclude the influence of any impurities from the carbon cloth. It is generally believed that at elevated temperatures the MoO<sub>x</sub> vapor generated from MoO<sub>3</sub> powder reacts with sulfur vapor and being sulfurized to form monolayer MoS<sub>2</sub> on the collecting substrates, therefore the reduction of MoO<sub>x</sub> is a critical step for the MoS<sub>2</sub> formation<sup>38</sup>.

Accordingly we further investigated the surface reaction of carbon cloth with MoO<sub>x</sub> during MoS<sub>2</sub> synthesis. Figure 1 (h) and (i) show the Scanning Electron Microscope (SEM) images of the carbon cloth surface before and after the growth. The pristine carbon cloth is manufactured in bundles of thousands of tiny fibers, and woven onto a fabric roll. After growth, the surface of carbon cloth facing the MoO<sub>3</sub> precursor are fully covered by micro size flakes or large crystals, as displayed in Fig. 1 (j) and (k). Figure 1 (l) compares the Raman spectrums from carbon cloth before and after the CVD process. These micro crystals deposited on the carbon cloth surface show strong Raman peaks and the carbon peaks

at around 1300 and 1600  $\text{cm}^{-1}$  become comparatively weaker. According to the literature, the additional Raman peaks obtained after CVD process belongs to  $\text{MoO}_2$ <sup>47,48</sup>. However, there are no detectable  $\text{MoS}_2$  Raman peaks from carbon cloth.

The forming of  $\text{MoO}_2$  crystals on the surface of carbon cloth suggests carbon is more reductive under elevated temperature to react with vapor phase  $\text{MoO}_3$ . In our experiments, the carbon cloth directly contacted with  $\text{MoO}_3$  powder, thus no sufficient sulfur vapor can penetrate through the carbon layer to react with the precursor underneath. In other words, the additional carbon layer helped to create an abrupt  $\text{MoO}_{3-x}$  concentration change between the top and bottom layer of the carbon cloth. It is well known that the reduction of  $\text{MoO}_{3-x}$  by sulfur can produce  $\text{MoO}_2$  and further sulfurization gives  $\text{MoS}_2$  layers<sup>27,29,30,37</sup>. Therefore, it is likely that during the growing process where the carbon layer provides a more steady and sustainable flow of  $\text{MoO}_{3-x}$  ( $x > 1$ ) and results a more constant ratio of Mo and S to form stoichiometry  $\text{MoS}_2$  crystallites. The reduction capability of carbon cloth was also compared with other form of carbon such as well crystallized highly ordered pyrolytic graphite (HOPG). Our results suggest well crystallized carbon, such as HOPG is more inert in the reaction with  $\text{MoO}_3$  during the growth (See the Supporting Data). The Raman spectra in Fig. 1 (l) show a strong D band at around 1300  $\text{cm}^{-1}$ , which indicates the defective nature of carbon cloths. The defective nature of carbon cloth makes it more reactive and attractive for molybdenum source with a large interacting surface with  $\text{MoO}_{3-x}$ . Thus these carbon fibers assist the reduction of  $\text{MoO}_{3-x}$  for  $\text{MoS}_2$  growth with improved reactivity and efficiency.

Recently, Kong *et al.* reported vertically aligned  $\text{MoS}_2$  and molybdenum diselenide ( $\text{MoSe}_2$ ) layers can be produced by a rapid sulfurization/selenization process at 550 °C<sup>49</sup>. It is suggested that the formation of vertically aligned TMD layers is driven by a kinetic process. When the growth is limited by the diffusion of sulfur/selenium, due to the anisotropic structure of TMD layers, it is much faster for sulfur/selenium to diffuse along the van der Waals gaps. Therefore, the TMD layers naturally oriented perpendicular to the film, exposing van der Waals gaps for fast reactions<sup>49</sup>. The assisted reduction process of  $\text{MoO}_{3-x}$  by carbon based materials is likely to alter the growth rate and thus provides a way to tune the surface structure of TMD layers.

In order to better understand the growth mechanism and further develop a method which is capable of engineering the surface structure of  $\text{MoS}_2$  layers in a controlled manner. Carbon based materials were deposited directly on the growth substrates to tune the local growth condition. Graphene oxide (GO) prepared by modified Hummers method is generally accepted as a defective form of carbon and GO flakes with abundant function groups also show similar Raman feature with the carbon cloth used in our study (See Supporting Data). Therefore, GO was chosen to reveal the reaction between carbon and  $\text{MoO}_{3-x}$  and its effects on the crystallization of  $\text{MoS}_2$  crystallites. To investigate the growth mechanism and reveal the role of carbon promoter during  $\text{MoS}_2$  formation, GO dispersed in DI water was drop casted on cleaned Si wafer with 300 nm  $\text{SiO}_2$  top layer. The GO casted substrates were carried into CVD furnace and  $\text{MoS}_2$  growth was then carried out. Figure 2 (a), (b) and (c) show the optical image of GO coated  $\text{SiO}_2/\text{Si}$  wafer after growth. The color contrast is due to the different layer thickness of deposited materials. Flakes with irregular shape can be found among the single layer  $\text{MoS}_2$ . We chose a location that fully covered with  $\text{MoS}_2$  monolayer and GO flakes can be found distributed among the mono layer  $\text{MoS}_2$ . The Raman measurement clearly shows the distribution of monolayer and few-layer  $\text{MoS}_2$ . Spectrum in Fig. 2 (d) shows a typical comparison of PL and Raman peak intensity taken from an irregular shaped few layer  $\text{MoS}_2$  and its surrounding. Note that the Raman peak of GO becomes very weak after CVD synthesis. The mapping in Fig. 2 (e) and (f) displays the peak intensity distribution on the sample surface. Moreover, it is worthy to mention that for the typical growth, most of the  $\text{SiO}_2/\text{Si}$  surface were covered with triangular monolayer  $\text{MoS}_2$  crystallites or  $\text{MoS}_2$  film. Meanwhile, all the  $\text{MoS}_2$  Raman peaks taken from the GO surface have a large  $E_{2g}$  to  $A_{1g}$  peak distance suggesting they are few-layers (see supporting information). These results are solid evidence that the GO tends to attract and promote  $\text{MoS}_2$  growth. We also noticed that without sulfur supply, monolayer GO is more reactive and can be totally etched away by  $\text{MoO}_3$  vapor (see supporting information) which also suggests the carbon  $\text{MoO}_3$  reduction reaction takes place during the growth.

**Flower-shape  $\text{MoS}_2$  growth, characterization and application.** Since it was reported that sulfurization process largely affects the layer orientations in the synthesized chalcogenide<sup>49-51</sup>. As discussed, at high temperatures, carbon can dramatically enhance the reduction of  $\text{MoO}_3$ , thus promote the formation of  $\text{MoO}_{3-x}$  ( $x > 1$ ) to react with sulfur vapor which further converts to  $\text{MoS}_2$  layers. Thereby under monolayer  $\text{MoS}_2$  growth condition, the introduction of additional carbon materials is likely to create a localized sulfur diffusion limited process for  $\text{MoS}_2$  growth. In order to investigate the effect of carbon on the layer orientations of synthesized chalcogenides, we intentionally apply more carbon based materials by utilizing filtrated GO thin film as the growth template, and all the other growth conditions were kept unchanged. The as grown samples possess a dramatically different morphology as shown in Fig. 3 (a) and (b). Interestingly, the synthesized  $\text{MoS}_2$  layers tend to form in a micrometer flower shape as illustrated in Fig. 3 (c). Figure 3 (d) displays the energy-dispersive X-ray spectroscopy (EDS) mapping characterization, which confirms the chemical composition of the flower shape structure.

Further structural characterizations using transmission electron microscopy (TEM) provide additional insights into  $\text{MoS}_2/\text{GO}$  composite film. Figure 4 shows the typical TEM images of  $\text{MoS}_2/\text{GO}$  film. Figure 4 (a) displays a low magnification TEM image, where the  $\text{MoS}_2$  layers show a darker color contrast

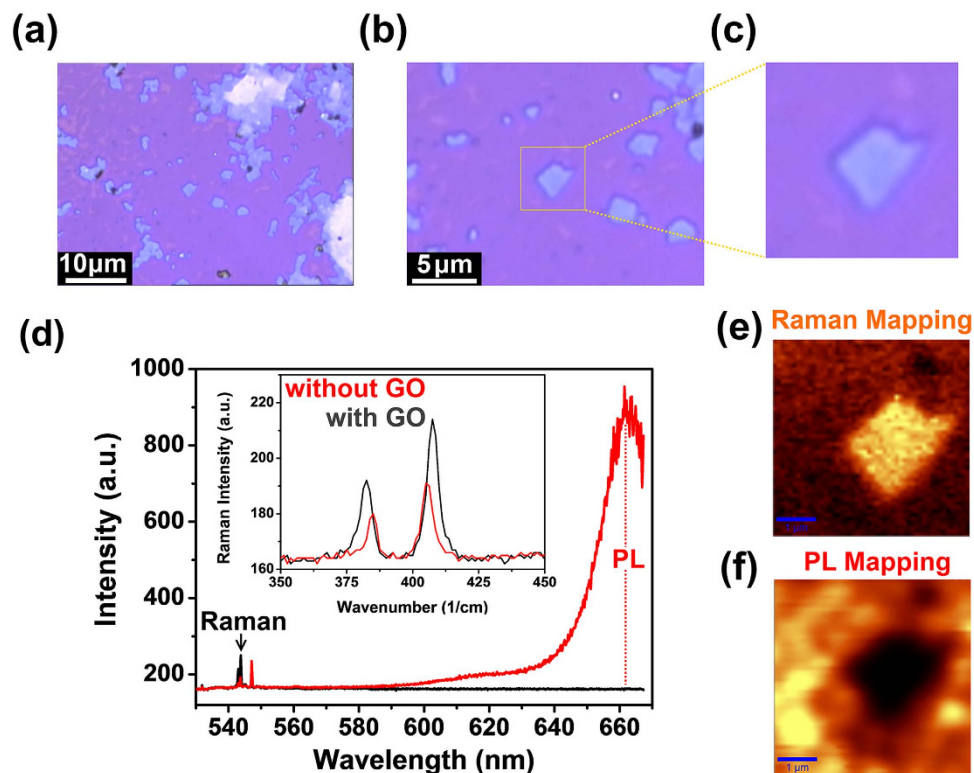


**Figure 2.** (a), (b) and (c) present the optical microscope images of GO coated  $\text{SiO}_2/\text{Si}$  substrates after CVD synthesis taken under various magnifications. (d) Typical PL and Raman spectrums taken from monolayer and few layer  $\text{MoS}_2$  regions. (e) and (f) are the corresponding Raman and PL maps in Fig. (c), the rectangular shape present a few layer  $\text{MoS}_2$  with monolayer  $\text{MoS}_2$  surrounding it.

on GO thin film. Figure 4 (b) exhibits a high-resolution TEM (HRTEM) image taken along the edge part of these composites. Stripe-like grains with  $\sim 10$  nm in length and several nanometers in width were found, however these grains are densely packed and overlapped with each other preventing an accurate lattice structure analysis. In Fig. 4 (c), the HRTEM image on a single grain reveals individual atomic planes ordered in the S–Mo–S sequence to form each layer. The carbon surface with a lighter color contrast under TEM was confirmed to be graphene by performing the selected area electron diffraction (SEAD) and the FFT confirms the hexagonal arrangement of S–Mo–S atoms. As shown in Fig. 4 (d), both the HRTEM image and fast Fourier transform (FFT) pattern reveal that  $\text{MoS}_2$  flakes grown on GO retain the crystal symmetry with the lattice constant  $\sim 0.32$  nm. Both of the EDS and TEM analysis suggests the  $\text{MoS}_2$  layers tend to form a layered flower-shape structure on GO substrates compared to monolayer in plan growth on  $\text{SiO}_2/\text{Si}$  substrates. The morphology change is likely due to the promoted conversion rate of  $\text{MoO}_{3-x}$ , where the chemical conversion occurs much faster than the diffusion of sulfur gas into the film, forcing the  $\text{MoS}_2$  layers naturally oriented perpendicular to the growth substrates, exposing van der Waals gaps for fast reaction<sup>49</sup>.

As a proof-of-concept application, the electrochemical property of the  $\text{MoS}_2/\text{GO}$  composite as an anode material of a Lithium ion battery (LIB) was further investigated by galvanostatic discharge/charge and cyclic voltammetry (CV) measurements. The measurement was based on a half-cell configuration as shown in the supporting materials. Figure 5 (a) illustrates the first, second and third discharge/charge voltage profiles of the flower shape  $\text{MoS}_2/\text{GO}$  composite electrode grown by CVD method. The test were carried out in the voltage range from 0.01 to 3V (vs.  $\text{Li}/\text{Li}^+$ ). The initial discharge and charge capacities were measured to be 1612 and 1149  $\text{mAhg}^{-1}$ , respectively, with a corresponding initial Coulombic efficiency of 71.3%. The irreversible capacity loss for the first cycle could be mainly attributed to the electrolyte decomposition and inevitable formation of the solid electrolyte interface (SEI), which are commonly observed for nanosized anode materials<sup>13</sup>. The second and third cycles show a decreased capacity but with a much higher Coulombic efficiency of 93.8% and 95.3%, respectively. In the first discharge process, the initial discharge capacity between 2.0 to 1.5V can be attributed to the reaction of residual carbon surface functional group and the lithium insertion to  $\text{MoS}_2$  which forms  $\text{Li}_x\text{MoS}_2$ . The following capacity between 1.0 to 0.5V can be attributed to the conversion reaction process of  $\text{MoS}_2$ , where the metal sulfide reacts with lithium ions forming metal nanoparticles and insoluble  $\text{Li}_2\text{S}$  matrix,  $\text{MoS}_2 + 4\text{Li}^+ + 4\text{e}^- \rightarrow \text{Mo} + 2\text{Li}_2\text{S}$ <sup>14</sup>. The formation of a SEI and the gel-like polymeric layer on the surface of the active materials contribute to the sloping plateau at the lower voltage region ( $< 0.5$  V). In the charge

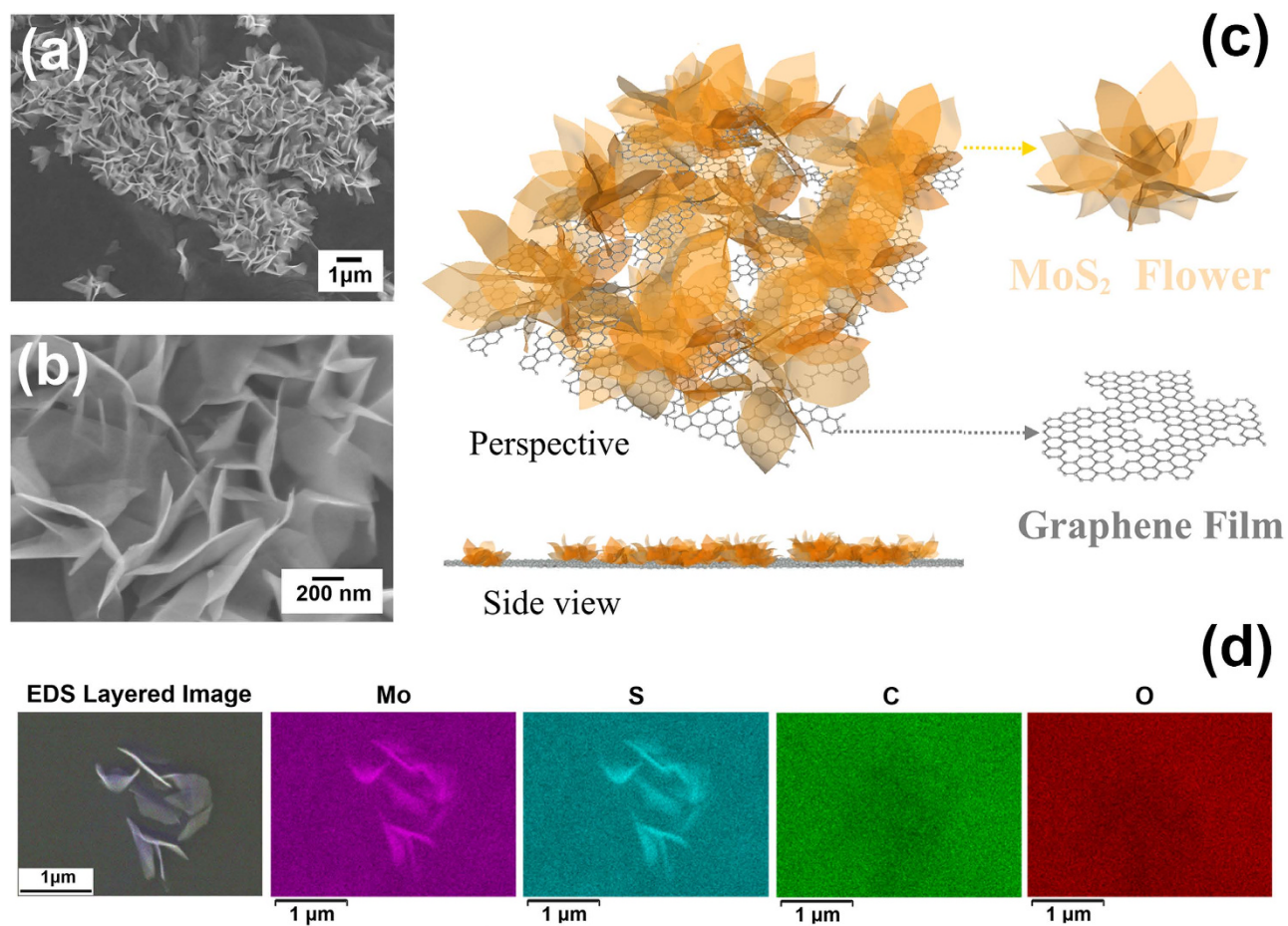


**Figure 3.** (a) and (b) show the SEM images of samples obtained by using GO thin film as growth templates. (c) Schematic illustration of flower-shape  $\text{MoS}_2$  grown on GO thin film. (d) EDS mapping of a layered structure region. The EDS intensity maps confirm the chemical composition of these layered structures to be  $\text{MoS}_2$ .

process, the plateau at  $\sim 1.3$  V and the sloping region above 2.2 V can be attributed to the reverse reaction process, where oxidation of Mo particles to  $\text{MoS}_2$  and the conversion of  $\text{Li}_2\text{S}$  to S and  $\text{Li}^+$  occur<sup>14,52,53</sup>. It is noted that the lithium extraction from the  $\text{Li}_x\text{MoS}_2$  phase should also be considered.

To further clarify the electrochemical process of  $\text{MoS}_2/\text{GO}$  composite, cyclic voltammogram (CV) measurements of the first three cycles in the voltage range of 0.01–3.0 V at a scan rate of  $0.1 \text{ mV s}^{-1}$  were carried out as shown in Fig. 5 (b). In the initial cycle, two reduction peaks at 1.1 and 0.5 V were observed, which can be attributed to the formation of  $\text{Li}_x\text{MoS}_2$  and the conversion reaction that leading to Mo metal nanoparticles embedded in a  $\text{Li}_2\text{S}$  matrix. In the reverse anodic scan, the oxidation peak at  $\sim 1.4$  V can be partly attributed to the oxidation of Mo to  $\text{MoS}_2$  and the peak at  $\sim 2.3$  V can be assigned to the oxidation of  $\text{Li}_2\text{S}$  to S. In the 2<sup>nd</sup> CV scan, the reduction peak at 0.9 V can be attributed to the Li insertion into  $\text{MoS}_2$  lattice to form  $\text{Li}_x\text{MoS}_2$ . The weak reduction peak at ca. 2.1 V indicates the formation of  $\text{Li}_2\text{S}$ . In the anodic sweeps, the oxidation peaks at 1.4 V and 2.3 V correspond to the extraction of  $\text{Li}^+$  from  $\text{Li}_x\text{MoS}_2$  lattice and the oxidation of  $\text{Li}_2\text{S}$ , respectively. The results are in agreement with the above lithiation and delithiation profiles.

The  $\text{MoS}_2/\text{GO}$  composites also possess outstanding high-rate performance. Figure 5 (c) shows cycle performance of the composite electrodes under high current density of 1000 and  $2000 \text{ mA g}^{-1}$ . The initial discharge and reversible capacities are ca. 1484 and  $779 \text{ mAh g}^{-1}$ , respectively, at  $1000 \text{ mA g}^{-1}$ , which retain ca. 68% of capacities at  $100 \text{ mA g}^{-1}$  (see supporting information). After the initial 36 cycles, the specific capacity slightly decreased to  $542 \text{ mAh g}^{-1}$ . However, a subsequent increase of specific capacity was observed for  $\text{MoS}_2/\text{GO}$  composites, which should be attributed to the gradual activation of the electrode during lithiation and delithiation and a formation of gel-like film resulting from decomposition of the electrolyte at a low voltage. Due to the vertical structure of  $\text{MoS}_2$ , the  $\text{Li}^+$  could get sufficient contact with the atomic layers of  $\text{MoS}_2$ . As a result, excellent electrochemical performance was achieved for vertical grown  $\text{MoS}_2$  and GO film. The reversible capacity can retain  $776 \text{ mAh g}^{-1}$  even after a long cycling

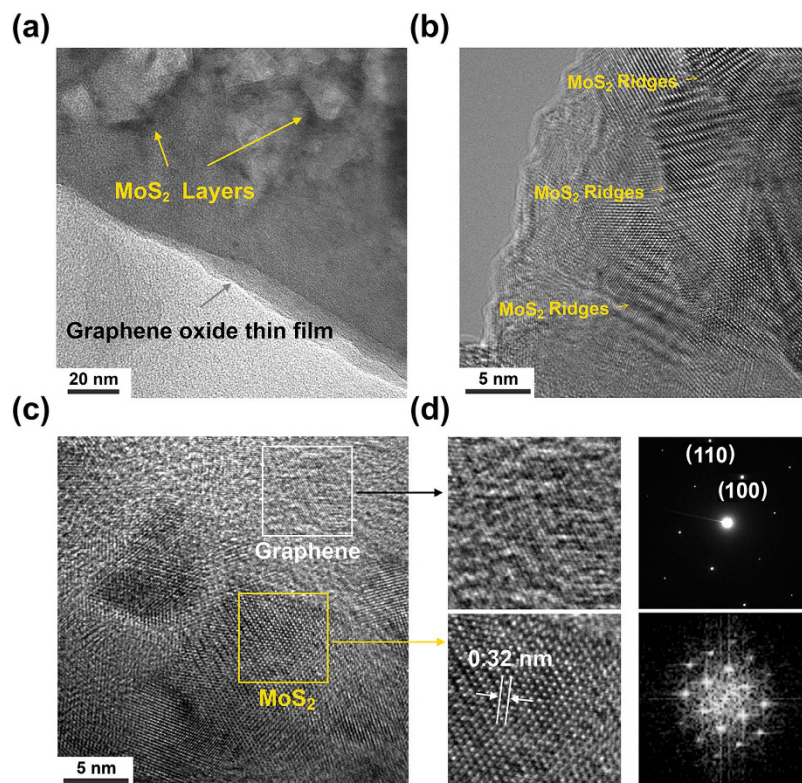


**Figure 4.** (a) and (b) TEM images of MoS<sub>2</sub>/GO composite under different magnifications; (c) HRTEM image shows both graphene and MoS<sub>2</sub> regions; (d) enlarged HRTEM images display the corresponding carbon and MoS<sub>2</sub> lattice structures. SAED in upper right confirms the background is graphene. FFT in the bottom right, suggests the hexagonal arrangement of S-Mo-S elements in MoS<sub>2</sub> layers.

period of 500 cycles. When the current density increases to 2000 mA g<sup>-1</sup>, the reversible capacity after 940 cycles can still retain ~727 mAh g<sup>-1</sup>, which is about 94% of that at 1000 mA g<sup>-1</sup>.

The MoS<sub>2</sub>/GO composites electrodes were further investigated by the electrochemical impedance spectroscopy measurement where the Nyquist plots of MoS<sub>2</sub>/GO composite and MoS<sub>2</sub>:GO (commercial MoS<sub>2</sub> and GO powder mixed in solution phase followed by freeze-dried to form a self-supporting film) powder blended electrode after 10 discharge/charge activation cycles are shown in Fig. 5 (d). The corresponding equivalent circuit is shown in the inset of Fig. 5 (d). The measurement indicates that the film resistance ( $R_f$ ) and charge-transfer resistance ( $R_{ct}$ ) of MoS<sub>2</sub>/GO are ca. 27 and 112  $\Omega$ , respectively. Both the  $R_f$  (106  $\Omega$ ) and  $R_{ct}$  (130  $\Omega$ ) of MoS<sub>2</sub>:GO mixture are much larger than those of MoS<sub>2</sub>/GO electrode. Since the MoS<sub>2</sub>/GO composites electrode possesses lower charge-transfer resistance, the charge transfer is lower than that of MoS<sub>2</sub>:GO blends. The significantly improved charge capacity of MoS<sub>2</sub>/GO composites could be attributed to the unique nanostructure of MoS<sub>2</sub> sheets on the surface of GO film. The vertical structured MoS<sub>2</sub> with extruding layers on GO has a much larger surface area, which provide more active sites during charging-discharging processes. In addition, lithium ions can be inserted/extracted into/out-of the vertical MoS<sub>2</sub> flakes from both sides of MoS<sub>2</sub>, leading to a quick lithiation and delithiation process even under a large current density, as shown in the schematic diagram in Fig. 5 (e). Therefore, the MoS<sub>2</sub>/GO composite electrodes show excellent rate performance.

## Conclusion

In conclusion, we propose a carbon promoted process to synthesize large-area and highly crystalline MoS<sub>2</sub> thin layers. The addition of carbon based materials during the high-temperature annealing drastically enhances the reduction of MoO<sub>3</sub> vapor, as evidenced by various spectroscopic and microscopic characterizations including Raman, PL, TEM, and SAED. In particular, using GO thin film as the growth template results in an edge-terminated layered chalcogenide films forming in a flower shaped MoS<sub>2</sub>/GO composite. These MoS<sub>2</sub> thin layers tend to orientate perpendicular to the growth substrate due to the sulfur diffusion limited process. The synthetic approach is simple and scalable, providing not only an easy but also efficient way to manipulate the structure of chalcogenide films. The unique structure paves the way to use the edges of layered materials more effectively.



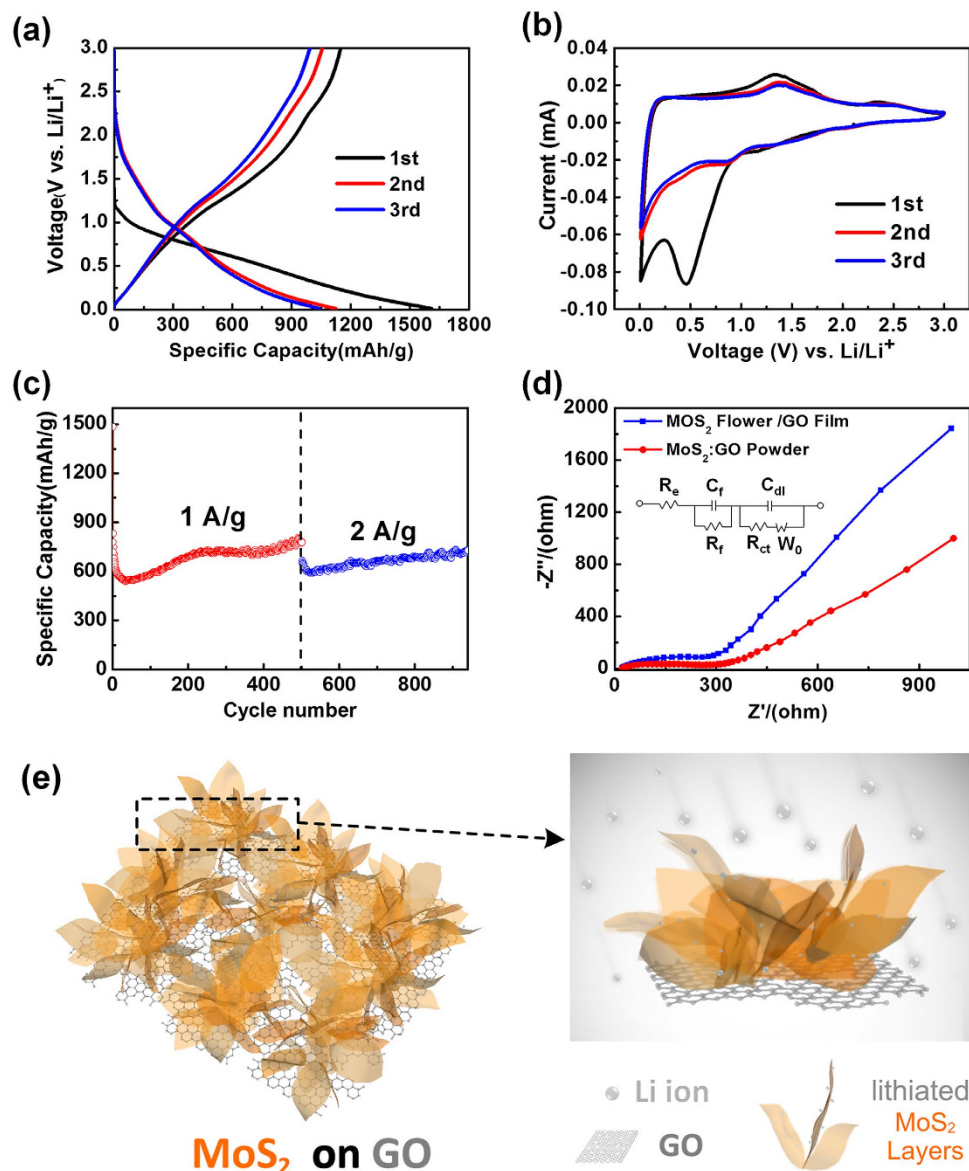


**Figure 5.** (a) Charge-discharge curves of MoS<sub>2</sub>/GO composites at current density of 100 mA g<sup>-1</sup>; (b) Representative cyclic voltammograms of MoS<sub>2</sub>/GO composite at the first 3 cycles between 0.01 V and 3.0 V at scan rate of 0.1 mV s<sup>-1</sup>; (c) The cycling performance of MoS<sub>2</sub>/GO composite at various current densities of 1 A g<sup>-1</sup> and 2 A g<sup>-1</sup> (d) Nyquist plots of MoS<sub>2</sub>/GO composite and MoS<sub>2</sub>/GO powder blended electrode after 10 discharge/charge activation cycles. Inset shows the equivalent circuit model used for the fittings and the corresponding values are shown in Table 1. (e) Schematic illustration of the surface structure of MoS<sub>2</sub>/GO composite for high current density lithium storage.

Sample	R <sub>e</sub> (Ω)	R <sub>f</sub> (Ω)	R <sub>ct</sub> (Ω)
MoS <sub>2</sub> /GO powder	28	106	130
MoS <sub>2</sub> flower/GO film	19	27	112

**Table 1.** Fitting results of the EIS curves in Fig. 5 (d) using the equivalent circuit.

## References

- Chhowalla, M. *et al.* The chemistry of two-dimensional layered transition metal dichalcogenide nanosheets. *Nat Chem* **5**, 263–275 (2013).
- Huang, X., Zeng, Z. & Zhang, H. Metal dichalcogenide nanosheets: preparation, properties and applications. *Chem. Soc. Rev.* **42**, 1934–1946 (2013).
- Radisavljevic, B., Radenovic, A., Brivio, J., Giacometti, V. & Kis, A. Single-layer MoS<sub>2</sub> transistors. *Nat Nano* **6**, 147–150 (2011).

4. Wang, H. *et al.* Integrated Circuits Based on Bilayer MoS<sub>2</sub> Transistors. *Nano Lett.* **12**, 4674–4680 (2012).
5. Lee, G.-H. *et al.* Flexible and Transparent MoS<sub>2</sub> Field-Effect Transistors on Hexagonal Boron Nitride-Graphene Heterostructures. *ACS Nano* **7**, 7931–7936 (2013).
6. Pu, J. *et al.* Highly Flexible MoS<sub>2</sub> Thin-Film Transistors with Ion Gel Dielectrics. *Nano Lett.* **12**, 4013–4017 (2012).
7. Mai, C. *et al.* Many-Body Effects in Valleytronics: Direct Measurement of Valley Lifetimes in Single-Layer MoS<sub>2</sub>. *Nano Lett.* **14**, 202–206 (2013).
8. Ji, Q. *et al.* Epitaxial Monolayer MoS<sub>2</sub> on Mica with Novel Photoluminescence. *Nano Lett.* **13**, 3870–3877 (2013).
9. Chang, Y.-H. *et al.* Three-Dimensional Molybdenum Sulfide Sponges for Electrocatalytic Water Splitting. *Small* **10**, 895–900 (2014).
10. Chang, Y.-H. *et al.* Highly Efficient Electrocatalytic Hydrogen Production by MoS<sub>x</sub> Grown on Graphene-Protected 3D Ni Foams. *Adv. Mater.* **25**, 756–760 (2013).
11. Wang, L. *et al.* Functionalized MoS<sub>2</sub> Nanosheet-Based Field-Effect Biosensor for Label-Free Sensitive Detection of Cancer Marker Proteins in Solution. *Small* **10**, 1101–1105 (2014).
12. Loan, P. T. K. *et al.* Graphene/MoS<sub>2</sub> Heterostructures for Ultrasensitive Detection of DNA Hybridisation. *Adv. Mater.* **26**, 4838–4844 (2014).
13. Cao, X. *et al.* Preparation of MoS<sub>2</sub>-Coated Three-Dimensional Graphene Networks for High-Performance Anode Material in Lithium-Ion Batteries. *Small* **9**, 3433–3438 (2013).
14. Shi, Y. *et al.* Self-assembly of hierarchical MoS<sub>x</sub>/CNT nanocomposites (2 < x < 3): towards high performance anode materials for lithium ion batteries. *Sci. Rep.* **3** (2013).
15. Wang, Y. *et al.* Pre-lithiation of onion-like carbon/MoS<sub>2</sub> nano-urchin anodes for high-performance rechargeable lithium ion batteries. *Nanoscale* **6**, 8884–8890 (2014).
16. Salvatore, G. A. *et al.* Fabrication and Transfer of Flexible Few-Layers MoS<sub>2</sub> Thin Film Transistors to Any Arbitrary Substrate. *ACS Nano* **7**, 8809–8815 (2013).
17. Shi, Y. *et al.* Selective Decoration of Au Nanoparticles on Monolayer MoS<sub>2</sub> Single Crystals. *Sci. Rep.* **3** (2013).
18. Roy, K. *et al.* Graphene-MoS<sub>2</sub> hybrid structures for multifunctional photoresponsive memory devices. *Nat Nano* **8**, 826–830 (2013).
19. Zhang, W. *et al.* Ultrahigh-Gain Photodetectors Based on Atomically Thin Graphene-MoS<sub>2</sub> Heterostructures. *Sci. Rep.* **4** (2014).
20. Wu, S. *et al.* Vapor–Solid Growth of High Optical Quality MoS<sub>2</sub> Monolayers with Near-Unity Valley Polarization. *ACS Nano* **7**, 2768–2772 (2013).
21. Su, S.-H. *et al.* Band Gap-Tunable Molybdenum Sulfide Selenide Monolayer Alloy. *Small* **10**, 2589–2594 (2014).
22. Mertens, J. *et al.* Excitons in a mirror: Formation of “optical bilayers” using MoS<sub>2</sub> monolayers on gold substrates. *Appl. Phys. Lett.* **104**, - (2014).
23. Kibsgaard, J., Chen, Z., Reinecke, B. N. & Jaramillo, T. F. Engineering the surface structure of MoS<sub>2</sub> to preferentially expose active edge sites for electrocatalysis. *Nat Mater* **11**, 963–969 (2012).
24. Zhan, Y., Liu, Z., Najmaei, S., Ajayan, P. M. & Lou, J. Large-Area Vapor-Phase Growth and Characterization of MoS<sub>2</sub> Atomic Layers on a SiO<sub>2</sub> Substrate. *Small* **8**, 966–971 (2012).
25. Shi, Y. *et al.* van der Waals Epitaxy of MoS<sub>2</sub> Layers Using Graphene As Growth Templates. *Nano Lett.* **12**, 2784–2791 (2012).
26. Lin, Y.-C. *et al.* Wafer-scale MoS<sub>2</sub> thin layers prepared by MoO<sub>3</sub> sulfurization. *Nanoscale* **4**, 6637–6641 (2012).
27. van der Zande, A. M. *et al.* Grains and grain boundaries in highly crystalline monolayer molybdenum disulphide. *Nat Mater* **12**, 554–561 (2013).
28. Najmaei, S. *et al.* Vapour phase growth and grain boundary structure of molybdenum disulphide atomic layers. *Nat Mater* **12**, 754–759 (2013).
29. Lee, Y.-H. *et al.* Synthesis of Large-Area MoS<sub>2</sub> Atomic Layers with Chemical Vapor Deposition. *Adv. Mater.* **24**, 2320–2325 (2012).
30. Ling, X. *et al.* Role of the Seeding Promoter in MoS<sub>2</sub> Growth by Chemical Vapor Deposition. *Nano Lett.* **14**, 464–472 (2014).
31. Reina, A. *et al.* Large Area, Few-Layer Graphene Films on Arbitrary Substrates by Chemical Vapor Deposition. *Nano Lett.* **9**, 30–35 (2008).
32. Li, X. *et al.* Large-Area Graphene Single Crystals Grown by Low-Pressure Chemical Vapor Deposition of Methane on Copper. *J. Am. Chem. Soc.* **133**, 2816–2819 (2011).
33. Shi, Y. *et al.* Synthesis of Few-Layer Hexagonal Boron Nitride Thin Film by Chemical Vapor Deposition. *Nano Lett.* **10**, 4134–4139 (2010).
34. Kim, K. K. *et al.* Synthesis of Monolayer Hexagonal Boron Nitride on Cu Foil Using Chemical Vapor Deposition. *Nano Lett.* **12**, 161–166 (2011).
35. Liu, K.-K. *et al.* Growth of Large-Area and Highly Crystalline MoS<sub>2</sub> Thin Layers on Insulating Substrates. *Nano Lett.* **12**, 1538–1544 (2012).
36. Liu, K.-K. *et al.* Chemical Vapor Deposited MoS<sub>2</sub> Thin Layers and Their Applications. *ECS Transactions* **50**, 61–63 (2013).
37. Lee, Y.-H. *et al.* Synthesis and Transfer of Single-Layer Transition Metal Disulfides on Diverse Surfaces. *Nano Lett.* **13**, 1852–1857 (2013).
38. Wang, X., Feng, H., Wu, Y. & Jiao, L. Controlled Synthesis of Highly Crystalline MoS<sub>2</sub> Flakes by Chemical Vapor Deposition. *J. Am. Chem. Soc.* **135**, 5304–5307 (2013).
39. Ji, Q., Zhang, Y., Zhang, Y. & Liu, Z. Chemical vapour deposition of group-VIB metal dichalcogenide monolayers: engineered substrates from amorphous to single crystalline. *Chem. Soc. Rev.*, DOI: 10.1039/C1034cs00258j (2015).
40. Shi, Y., Li, H. & Li, L.-J. Recent advances in controlled synthesis of two-dimensional transition metal dichalcogenides via vapour deposition techniques. *Chem. Soc. Rev.*, DOI: 10.1039/c1034cs00256c (2015).
41. Schmidt, H. *et al.* Transport Properties of Monolayer MoS<sub>2</sub> Grown by Chemical Vapor Deposition. *Nano Lett.* **14**, 1909–1913 (2014).
42. Eda, G. *et al.* Photoluminescence from Chemically Exfoliated MoS<sub>2</sub>. *Nano Lett.* **11**, 5111–5116 (2011).
43. Splendiani, A. *et al.* Emerging Photoluminescence in Monolayer MoS<sub>2</sub>. *Nano Lett.* **10**, 1271–1275 (2010).
44. Li, H. *et al.* From Bulk to Monolayer MoS<sub>2</sub>: Evolution of Raman Scattering. *Adv. Funct. Mater.* **22**, 1385–1390 (2012).
45. Lee, C. *et al.* Anomalous Lattice Vibrations of Single- and Few-Layer MoS<sub>2</sub>. *ACS Nano* **4**, 2695–2700 (2010).
46. Li, S.-L. *et al.* Quantitative Raman Spectrum and Reliable Thickness Identification for Atomic Layers on Insulating Substrates. *ACS Nano* **6**, 7381–7388 (2012).
47. Camacho-López, M. A. *et al.* Micro-Raman study of the m-MoO<sub>2</sub> to α-MoO<sub>3</sub> transformation induced by cw-laser irradiation. *Opt. Mater.* **33**, 480–484 (2011).
48. Dieterle, M. & Mestl, G. Raman spectroscopy of molybdenum oxides Part II. Resonance Raman spectroscopic characterization of the molybdenum oxides Mo<sub>3</sub>O<sub>11</sub> and MoO<sub>2</sub>. *PCCP* **4**, 822–826 (2002).
49. Kong, D. *et al.* Synthesis of MoS<sub>2</sub> and MoSe<sub>2</sub> Films with Vertically Aligned Layers. *Nano Lett.* **13**, 1341–1347 (2013).
50. Jäger-Waldau, A., Lux-Steiner, M., Jäger-Waldau, R., Burkhardt, R. & Bucher, E. Composition and morphology of MoSe<sub>2</sub> thin films. *Thin Solid Films* **189**, 339–345 (1990).

51. Jäger-Waldau, A. *et al.* MoS<sub>2</sub> thin films prepared by sulphurization. *Appl. Surf. Sci.* **65-66**, 465–472 (1993).
52. Yang, L. *et al.* Hierarchical MoS<sub>2</sub>/Polyaniline Nanowires with Excellent Electrochemical Performance for Lithium-Ion Batteries. *Adv. Mater.* **25**, 1180–1184 (2013).
53. Gong, Y. *et al.* A Bottom-Up Approach to Build 3D Architectures from Nanosheets for Superior Lithium Storage. *Adv. Funct. Mater.* **24**, 125–130 (2014).

## Acknowledgements

This work was supported by SUTD-MIT international design center (IDC) grant.

## Author Contributions

Y. S. and H. Y. Y. designed research and analyzed data. Y. S., H. L. and J. I. W., carried out the material growth, synthesis and characterization. X. Z., H. S. and Y. W. performed the electrochemical measurement. H.Y. Y. supervised the project. All authors contributed to the writing and editing.

## Additional Information

**Supplementary information** accompanies this paper at <http://www.nature.com/srep>

**Competing financial interests:** The authors declare no competing financial interests.

**How to cite this article:** Shi, Y. *et al.* MoS<sub>2</sub> Surface Structure Tailoring *via* Carbonaceous Promoter. *Sci. Rep.* **5**, 10378; doi: 10.1038/srep10378 (2015).



This work is licensed under a Creative Commons Attribution 4.0 International License. The images or other third party material in this article are included in the article's Creative Commons license, unless indicated otherwise in the credit line; if the material is not included under the Creative Commons license, users will need to obtain permission from the license holder to reproduce the material. To view a copy of this license, visit <http://creativecommons.org/licenses/by/4.0/>

# SCIENTIFIC REPORTS

**OPEN**

## Corrigendum: MoS<sub>2</sub> Surface Structure Tailoring *via* Carbonaceous Promoter

Yumeng Shi, Henan Li, Jen It Wong, Xiaoting Zhang, Ye Wang, Huaihe Song & Hui Ying Yang

*Scientific Reports* 5:10378; doi: 10.1038/srep10378; published online 21 May 2015; updated on 20 January 2016

The Acknowledgements section is incomplete.

“This work was supported by SUTD-MIT international design center (IDC) grant.”

should read:

“This work was supported by SUTD-MIT international design center (IDC) grant and SUTD Temasek Seed funding (IGDSS1402031).”



This work is licensed under a Creative Commons Attribution 4.0 International License. The images or other third party material in this article are included in the article's Creative Commons license, unless indicated otherwise in the credit line; if the material is not included under the Creative Commons license, users will need to obtain permission from the license holder to reproduce the material. To view a copy of this license, visit <http://creativecommons.org/licenses/by/4.0/>